Spin- and charge-ordering in oxygen-vacancy-ordered mixed-valence $Sr_4Fe_4O_{11}$

R. Vidya,* P. Ravindran, H. Fjellvåg, and A. Kjekshus
Department of Chemistry, University of Oslo, Box 1033 Blindern, N-0315 Oslo, Norway
(Received 14 December 2005; published 18 August 2006)

The structural, electronic, and magnetic properties of the oxygen-vacancy-ordered mixed-valence $Sr_4Fe_4O_{11}$ phase have been investigated using spin-polarized electronic-structure total-energy calculations. The optimized structural parameters obtained from accurate total-energy calculations are found to be in very good agreement with low-temperature neutron-diffraction findings. Among the different spin configurations considered for $Sr_4Fe_4O_{11}$, the *G*-type antiferromagnetic configuration is found to represent the magnetic ground state. The calculations show finite magnetic moments at both Fe sites, and this is against the conclusions arrived at from Mössbauer spectroscopy and low-temperature powder neutron-diffraction measurements, but consistent with the results from magnetization measurements. The present study clearly show that one of the magnetic sublattices is frustrated and hence $Sr_4Fe_4O_{11}$ can be considered as a phase-separated system with one phase in the *G*-type antiferromagnetic state and the other in a spin-glass-like state. Our theoretical results show unambiguously that Fe atoms with the square pyramidal environment have a lower oxidation state than that in the octahedral coordination. However, the presence of a covalent interaction between Fe and the neighboring oxygen atoms makes the actual oxidation state considerably smaller than the formal oxidation state of 3+ and 4+ for square-pyramidal and octahedral coordination, respectively. $Sr_4Fe_4O_{11}$ is found to be semiconducting in the antiferromagnetic ground state.

DOI: 10.1103/PhysRevB.74.054422 PACS number(s): 75.50.Ee, 71.20.Ps, 78.20.Ci

I. INTRODUCTION

Perovskite-type oxides exhibiting ionic or mixed electronic-ionic conductivity are of considerable interest for potential applications in high-temperature electrochemical devices, e.g., as electrodes for high-temperature solid-oxide fuel cells, sensor materials, membranes separating oxygen from air, and catalyst for the conversion of hydrocarbons.[1–7] One of the most essential features of such materials is the high oxygen mobility, and another attraction is the catalytic activity of oxygen vacancies. However, the oxygen mobility usually drops appreciably at temperatures below ~600–800 °C and hence many, at first sight, seemingly promising materials turn out to be unsuitable for practical purposes. Therefore, the development of oxygen ionic conductors that retain appreciable oxygen mobility at ambient operating temperatures is of considerable interest. Since it is documented[8] that oxide ion conductivity is closely related to the ordering of oxygen vacancies in the crystal structure, it seems worthwhile to look more closely at the properties of oxygen-deficient perovskites.

The high-temperature phase $SrFeO_{3-x}$ $(2.5 \leqslant x \leqslant 3.0)$ exhibits appreciable mixed electronic and ionic conductivity, and the materials derived from this phase are considered to be of potential interest[9] for applications in many of the device categories mentioned above. From the scientific point of view, it is vital to explore the properties of phases with different oxygen stoichiometry as they form different structural distortions, exotic valences, spin, charge, orbital ordering, etc.

The orbital distribution of the *d* electrons of higher-valence Fe species is very versatile, changing not only with the kind and amount of other constituents (in particular alkali, alkaline-earth, or rare-earth elements) but also temperature as, e.g., observed for $Ca_{1-x}Sr_xFeO_3$ and $Sr_{1-x}La_xFeO_3$.[10] Another influential factor is the oxygen content as revealed for the $SrFeO_{3-x}$ (Ref. 9), $LaBaMn_2O_{5+\delta}$ (Ref. 11), and $YBaMn_2O_{5+\delta}$ (Ref. 12) phases. Oxygen deficiency formally increases the number of electrons per Fe atom and modifies (at least locally) the electron exchange between Fe atoms. Subsequently it perturbs the electronic band structure and varies the band filling of the transition-metal atom and also the structural arrangement simultaneously.

The preparation and characterization of oxygen-deficient specimens of $SrFeO_{3-x}$ have been subjected to numerous studies.[9,13–15] One of the curiosities which is commonly associated with the $SrFeO_{3-x}$ phase (more specifically with the highly electropositive element Sr) is the occurrence of Fe in a rare, formal oxidation state of 4+ and a wide range of oxygen nonstoichiometry. Systematic studies[13,14] have established the existence of a series of ordered Ruddlesden-Popper-type phases $Sr_nFe_nO_{3n-1}$ with $n=\infty$, 8, 4, and 2 corresponding to the formulas $SrFeO_3$, $SrFeO_{2.875}$ ($Sr_8Fe_8O_{23}$), $SrFeO_{2.75}$ ($Sr_4Fe_4O_{11}$), and $SrFeO_{2.5}$ ($Sr_2Fe_2O_5$), respectively. Hence the variable-valence phase $SrFeO_{3-x}$ may provide an instructive model system for a closer examination of the effects of oxygen-vacancy ordering on structure, magnetism, and electronic properties.

The oxygen-deficient end member $Sr_2Fe_2O_5$ is claimed[16] to exhibit well-behaved Fe^{3+} cations at both tetrahedral and octahedral coordination of an orthorhombic oxygen-vacancy-ordered structure[17] and it is an antiferromagnetic (AF) Mott-type insulator. The other end phase $SrFeO_3$ possesses, as mentioned, an unusually high Fe^{4+} oxidation state according to a pure ionic model. The structure is of the regular cubic perovskite type, the magnetic ordering is of the helical-AF type, and this phase exhibits metallic conductivity.[18,19] Between these composition limits one finds the two above-mentioned intermediate phases with oxygen-vacancy ordering.[13–15,20,21] The $Sr_4Fe_4O_{11}$ variant is reported to take

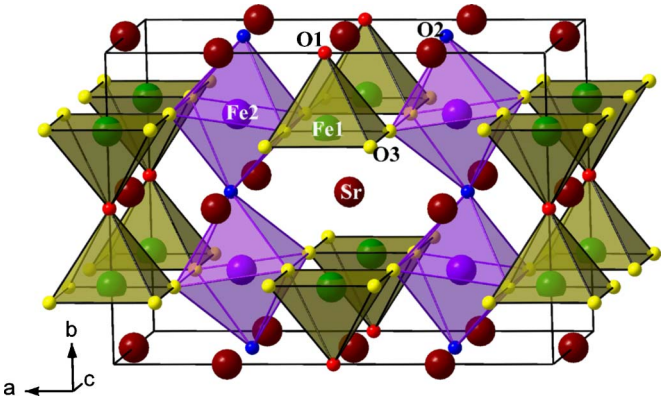

FIG. 1. (Color online) Crystal structure of $Sr_4Fe_4O_{11}$. $Fe(1)^s$ and $Fe(2)^o$ are in square-pyramidal and octahedral coordination, respectively.

an orthorhombic $2\sqrt{2}a_p \times 2a_p \times \sqrt{2}a_p$ (a_p refers to the lattice parameter of the cubic perovskite subcell) structure,[13] whereas $Sr_8Fe_8O_{23}$ has a tetragonal $2\sqrt{2}a_p \times 2\sqrt{2}a_p \times 2a_p$ structure. Both these variants exhibit AF ordering at low temperatures.

Tofield *et al.*[22] first reported that $Sr_4Fe_4O_{11}$ exists in a narrow single-phase region centered around the ideal stoichiometric composition 4:4:11. It is reported[23] to undergo a charge ordering (CO) transition below $T_{CO}=675$ K with equal amounts of Fe^{3+} and Fe^{4+} alternatively arranged in the lattice. $Sr_4Fe_4O_{11}$ is found[14,24] to be of the *G*-type AF with a Néel temperature (T_N) of 230 K. According to Mössbauer spectroscopic[14] and powder neutron diffraction[24] (PND) measurements, one Fe site forms a long-range AF arrangement. At present it is not known whether the other Fe sublattice forms a spin-glass-like configuration below T_N, remains paramagnetic, or possibly undergoes a separate spin-ordering (SO) transition at very low temperatures (notably below 4.2 K). In order to settle some of these issues accurate electronic structure studies are highly desirable and this demand was one of the motivations for the present study.

The hitherto conducted structural studies have clearly indicated that the Fe atoms alternatively occupy square pyramidal [$Fe(1)^s$] and octahedral [$Fe(2)^o$] sites in $Sr_4Fe_4O_{11}$. However, there is strong disagreement on the assignment of valence and spin states to the crystallographically different Fe atoms. From the calculated electronic structure and magnetic properties our study aims at resolving this controversy.

II. STRUCTURAL ASPECTS

The crystal structure of $Sr_4Fe_4O_{11}$ (Fig. 1) can be visualized as an oxygen-vacancy-ordered perovskitelike superstructure. It consists of one-dimensional chains of vertex-linked $Fe(2)O_6^o$ units cross-linked by $[Fe(1)O_5^s]_2$ "bow-tie" dimer units. The oxygen vacancies are ordered into strings of vacancies alternating with oxide ions along the [110] direction of the perovskite subcell. The interplane ordering is such that the structure contains equal amounts of Fe in square-pyramidal and octahedral coordination to the oxygen atoms.

The most prominent feature of this vacancy-ordered structure is the appearance of "one-dimensional channels" of apex-sharing $Fe(2)O_6^o$ units along the *b* direction (see Fig. 1). In planes parallel to *ac*, each of these octahedra is surrounded by four (corner-sharing) $Fe(1)O_5^s$ units. The $Fe(1)O_5^s$ unit consists of one O(1) and four O(3) atoms (the latter forming the base of the pyramid, labeling according to Hodges *et al.*[14]). The O(1) atom is shared by two neighboring Fe(1) atoms, and it is this configuration that forms the "bow-tie" unit. The Fe(1) atom is located close to the base of the pyramid. The octahedral surroundings of Fe(2) are formed by two O(2) and four O(3) atoms. The pyramids and octahedra share the O(3) atoms. For the $Fe(1)O_5^s$ units the increase in repulsion energy due to short O-O distances in the base is partly compensated by the relaxation effect of the longer separation between the O atoms in the base and apex. The $Fe(2)O_6^o$ units are compressed at the apex, a structural distortion introduced by the "bow-tie" configuration of the pyramids. However, this distortion causes only a tilting of the octahedra and does not change their shape (see Fig. 1).

III. COMPUTATIONAL DETAILS

A. Structural optimization

Two different structural arrangements (monoclinic $C2/m$ and orthorhombic $Cmmm$) are described for $Sr_4Fe_4O_{11}$ with full site occupancy,[14] and we have performed structural optimization for both in order to establish the ground-state structure. These calculations have been carried out utilizing the projected augmented plane-wave[25] (PAW) method as implemented in the Vienna *ab initio* simulation package[26] (VASP). The optimization of the atomic geometry was performed via a conjugate-gradient minimization of the total energy, using Hellmann-Feynman forces on the atoms and the stresses in the unit cell. The atomic coordinates and axial ratios are allowed to relax for different volumes of the unit cell. These parameters are changed iteratively so that the sum of the lattice energy and the electronic free energy converges to a minimum value. The electronic free energy is taken as the quantity to be minimized, and the total energy is calculated exactly for each set of atomic positions. The convergence minimum with respect to atomic shifts was assumed to have been attained when the energy difference between two successive iterations was less than 10^{-7} eV per unit cell and the forces acting on the atoms were less than 1 meV $Å^{-1}$. The generalized-gradient approximation[27] (GGA) was used to obtain accurate exchange and correlation energy for a particular atomic configuration. The calculations were carried out using a $4\times4\times4$ **k**-point Monkhorst-Pack grid, equivalent to 64 **k** points in the Brillouin zone. A plane-wave energy cutoff of 875 eV was used in all calculations since a high-energy cutoff was found[28] to be necessary in order to describe the nuclear and magnetic structures of complex oxides unambiguously.

B. FPLAPW calculation

In order to calculate the orbital-projected density of states (DOS) and energy-projected occupation density matrix we made use of the full-potential linearized-augmented plane-wave (FPLAPW) method as implemented in the WIEN2k

package[29] in a fully relativistic version with spin-orbit coupling. The FPLAPW approach divides space into an interstitial region (IR) and nonoverlapping muffin-tin (MT) spheres centered at the atomic sites. In the IR, the basis set consists of plane waves. Inside the MT spheres, the basis set is described by radial solutions of the one-particle Schrödinger equation (at fixed energies) and their energy derivatives multiplied by spherical harmonics. The charge densities and potentials inside the atomic spheres were represented by spherical harmonics up to $\ell=6$, whereas in the interstitial region these quantities were expanded in a Fourier series. Atomic-sphere radii (R_{MT}) of 2.3, 1.9, and 1.6 a.u. for Sr, Fe, and O, respectively, were used. The Brillouin zone (BZ) integration was carried out with a modified tetrahedron method,[25] and we used 75 **k** points in the irreducible wedge of the BZ for the DOS and total-energy calculation. Exchange and correlation effects are treated within the density-functional theory (DFT), using the GGA.[27]

IV. RESULTS AND DISCUSSIONS

Hodges *et al.*[14] tested different possible oxygen-ordering schemes for $Sr_4Fe_4O_{11}$ of which several gave almost equally good fits in Rietveld refinements of the PND data. However, all solutions except that based on space group *Cmmm* had to be disregarded owing to unacceptable short Fe-O distances. Our structural optimizations (according to the proposed structure models described in space groups $C2/m$ and *Cmmm*) came out with an energy gain of around 0.433 eV f.u.$^{-1}$ in favor of the variant specified in *Cmmm*. This confirms that the experimental studies have identified[14,15,24] the correct ground-state structure for $Sr_4Fe_4O_{11}$. For the optimized monoclinic structure, the calculated magnetic moments at the two Fe sites came out almost equal (differing only by $0.3\mu_B$) and also with no noticeable difference in the integrated charge for the Fe sites. These findings indicate that the CO is not pronounced in this structure, which, however, may represent a high-temperature phase with no charge ordering.

The reported unit-cell volume for $SrFeO_{3-x}$ at $x\approx0.25$ varies somewhat between different reports [458.41 ($x=0.247$) (Ref. 15), 462.21 ($x=0.27$) (Ref. 13), 462.59 ($x=0.26$) (Ref. 14), 463.05 ($x=0.29$) (Ref. 30), 463.15 Å^3 f.u.$^{-1}$ ($x=0.255$) (Ref. 23)]. This apparently significant variation may indicate a small homogeneity range for the $SrFeO_{2.75}$ ($Sr_4Fe_4O_{11}$) phase as suggested in the proposed phase diagrams.[13] The present optimized equilibrium volume (464.58 Å^3 f.u.$^{-1}$) for $Sr_4Fe_4O_{11}$ is somewhat larger than any of the experimental volumes but fully acceptable as good agreement (deviation less than 1.5%) for DFT calculations. The calculated unit-cell dimensions and positional parameters for the optimized ground-state structure according to space group *Cmmm* (Table I) are in very good agreement with the low-temperature PND data, once more exposing the predicting power of accurate DFT calculations even for quite complex systems.

To gain insight into the relations between the crystal structure and electronic and magnetic properties of $Sr_4Fe_4O_{11}$, a correct assignment of valence states to the crystallographically different Fe sites is critical. It therefore appears appropriate to give a brief account of the experimental findings for the valence- and spin-state situation for Fe in $Sr_4Fe_4O_{11}$. From low-temperature Mössbauer data it has been concluded[31] that only the Fe atoms in the formal 3+ state order magnetically below $T_N=220$ K. Room-temperature spectra comprise two symmetrical doublets of equal intensity,[30] which on the basis of the isomer shifts were assigned as Fe^{3+} ($\delta=0.35$ mm s^{-1}) and Fe^{4+} ($\delta=-0.08$ mm s^{-1}). Below T_N the spectra exhibit (hyperfine) magnetic splitting by an internal magnetic field of 46 T. The latter finding is interpreted[30] as indicative of a high-spin (HS) 3+ (d^5) state for iron.

TABLE I. Optimized structural parameters for the ground state of $Sr_4Fe_4O_{11}$ (space group *Cmmm*). Experimental data from Ref. 15 are given in parentheses.

Unit cell (Å or Å^3)	Atom	Site	(x, y, z)
$a=11.0372(10.9430)$	Sr(1)	2*d*	0, 0, 1/2 (0, 0, 1/2)
$b=7.6629(7.6795)$	Sr(2)	2*c*	1/2, 0, 1/2 (1/2, 0, 1/2)
$c=5.4930(5.4549)$	Sr(3)	4*g*	0.2421, 0, 0 (0.2400, 0, 0)
$V=464.58(458.41)$	Fe(1)	4*i*	0, 0.2468, 0 (0, 0.2410, 0)
	Fe(2)	4*f*	1/4, 1/4, 1/2 (1/4, 1/4, 1/2)
	O(1)	2*a*	0, 0, 0 (2*b*; 1/2, 0, 0)
	O(2)	4*h*	0.2284, 0, 1/2 (0.2320, 0, 1/2)
	O(3)	16*r*	0.1196, 0.2773, 0.2368 (0.1190, 0.2726, 0.2410)

Using the results from powder x-ray diffraction and Mössbauer spectroscopic measurements Takano *et al.*[21,32] concluded that $Fe(1)^s$ is in a 3+, HS state and $Fe(2)^o$ in a 4+, low-spin (LS) state on the additional assumption that $Fe(2)^o$ is subject to a residual disorder and only manifests itself in the broad background of the Mössbauer spectra. Fournes *et al.*,[23] on the other hand, concluded from room-temperature Mössbauer data that $Fe(2)^o$ is in the 3+, HS state (arguing with the isomer shift values for $SrFeO_{2.5}$ as reference substance) and $Fe(1)^s$ is in the 4+, HS state. Based on bond-valence sums Hodges *et al.*[14] concluded that $Fe(1)^s$ is in a 3+ state and $Fe(2)^o$ is in a 4+ state. The same authors argue that the $Fe(2)^o$ sublattice forms an AF-dominated magnetic structure, while the $Fe(1)^s$ sublattice is subject to conflicting magnetic superexchange interactions and does not exhibit cooperative magnetic order (remaining either as paramagnetic or developing a spin-glass-like moment arrangement). From the PND and magnetization-susceptibility data over the temperature range 1.5–293 K it has also been inferred[15] that $Fe(1)^s$ and $Fe(2)^o$ are in the 3+ and 4+ states, respectively, where Fe^{3+} orders antiferromagnetically below 232 K and Fe^{4+} forms a magnetically frustrated sublattice. This conclusion was arrived at by Schmidt *et al.*[15] who drew heavily from the accumulated knowledge on Sr-Fe-O compounds. From this summary it should be obvious that there are controversies on the interpretations of the so-called experimental facts regarding the assignment of valence and spin states to the different Fe sites in $Sr_4Fe_4O_{11}$.

It is interesting to analyze why different conclusions have been arrived at experimentally about spin- and valence-state

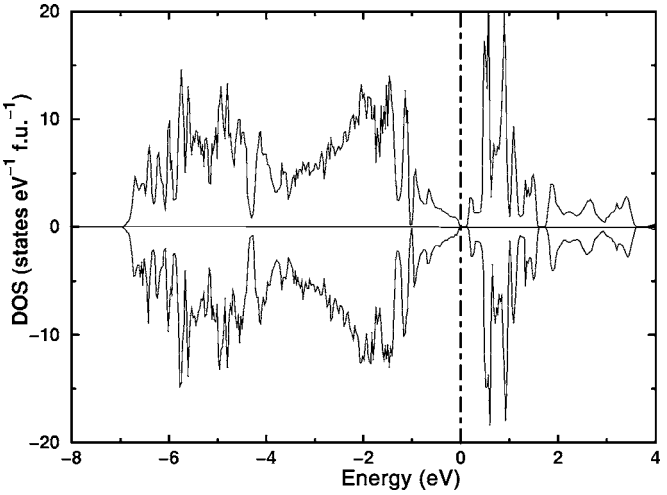

FIG. 2. Calculated total density of states (DOS) for $Sr_4Fe_4O_{11}$ in the ground-state *G*-AF configuration. The Fermi level is set to zero.

assignments to the different Fe sites. The Mössbauer spectroscopic assignments[15,31] draw heavily on isomer shift values for reference standards. However, these standards are not real standards in the sense that they provide a fixed value for each valence state of Fe. On the contrary, Mössbauer spectroscopy has a relatively broad range of isomer shift values at disposal for each valence state. This lack of precision is connected with the ambiguities one inevitably faces with every assignment of valence state. The bond-valence deductions are also based on the use of reference standards. Neither of these are universal standards, and simple single bond radii for Fe^{2+} and Fe^{3+} are certainly not fixed constant parameters. It gets even worse when it comes to Fe^{4+} where suitable reference compounds are scarcely available and the single-bond radius for Fe^{4+} is only estimated.[33]

Semiconducting behavior with an activation energy of 0.053 eV at 300 K has been reported for $SrFeO_{3-x}$ specimens with composition $x=0.28$ and 0.22.[34] Hence it can be anticipated that the transport properties of $SrFeO_{3-x}$ do not change drastically over a small compositional range. The total DOS given in Fig. 2 exposes that $Sr_4Fe_4O_{11}$ ($SrFeO_{2.75}$) is a semiconductor with a band gap of 0.13 eV. The observation of semiconducting behavior is consistent with experimental temperature-dependent electrical property measurements.[18,34] It should be remembered that density-functional calculations generally yield smaller band gaps than those obtained from experimental studies like optical measurements.

We now turn our attention to the assignment of the valence states for the Fe atoms from the DFT calculations. The calculated number of electrons at the $Fe(1)^s$ site is larger than that at the $Fe(2)^o$ site by around 0.5 electrons. This indicates that, as a coarse approximation $Fe(1)^s$ can be assigned the formal valence of 3+ and $Fe(2)^o$ accordingly as 4+. Now let us see why Fe in square-pyramid configuration should prefer the 3+ state rather than the 4+ state. The removal of an oxygen atom from an $Fe(2)O_6$ octahedron (present in the $SrFeO_3$ phase without oxygen vacancy) is formally the same as the addition of two electrons to the remaining structural framework. If one postulates that the defect is rectified mainly locally, one can imagine that, among the two electrons, one electron is used to convert Fe^{4+} into Fe^{3+} and the other electron participates in a bonding interaction with neighboring O sites. Moreover, as each $Fe(1)^s$ is surrounded by only five O compared to $Fe(2)^o$ with six O neighbors, $Fe(1)^s$ would prefer to have a lower oxidation state than that of $Fe(2)^o$ in an attempt to optimize the charge balance in the system.

The calculated magnetic moment at the $Fe(1)^s$ and $Fe(2)^o$ sites for the *G*-AF configuration are $2.82\mu_B$ and $3.44\mu_B$ per Fe atom, respectively. The calculated moment at the $Fe(2)^o$ site is in good agreement with the experimental moment from PND[15,24] (see Table III). The experimentally established AF ordering in $Sr_4Fe_4O_{11}$ concerns only the $Fe(2)^o$ atoms. However, neither PND nor Mössbauer spectroscopy was able to detect magnetic ordering of the moments at the $Fe(1)^s$ site, for reasons which will be discussed below. Neither of the Fe sites in $Sr_4Fe_4O_{11}$ has a perfect local cubic environment, and the electric field gradient at the $Fe(1)^s$ and $Fe(2)^o$ sites is of -1.56×10^{21} and -5.64×10^{21} V m^2, respectively. These calculated values are in accordance with the experimental observation of different quadrupole splittings for the two Fe sites in the Mössbauer spectra.[15]

The magnetic moment at the $Fe(2)^o$ site in $Sr_4Fe_4O_{11}$ can be compared with that in $SrFeO_3$ which has a cubic perovskite structure with an AF screw spin arrangement ($T_N=134$ K and a moment of $3.1\mu_B$/Fe at 4 K).[18,19] The Mössbauer spectroscopic data[16] for $SrFeO_3$ show an isomer shift of 0.05 mm/s and a magnetic hyperfine field (HF) of 33.1 T at 4 K which has been believed to be the typical values for Fe^{4+} in an octahedral environment. Our calculated magnetic moment for the $Fe(2)^o$ site ($3.53\mu_B$) in $Sr_4Fe_4O_{11}$ is found to be slightly larger than that in $SrFeO_3$. The larger moment value may be related to the oxygen vacancies present adjacent to the octahedra in the lattice, which is likely to weaken the Fe-O bonding interactions within the $Fe(2)O_6^o$ units. Hence relatively more electrons at the $Fe(2)^o$ site are allowed to participate in magnetism rather than in bonding. Consistent with this viewpoint the calculated Fe-O distance at the base of the octahedron in $Sr_4Fe_4O_{11}$ is larger than that in $SrFeO_3$ (2.05 vs 1.92 Å). Owing to the relatively large magnetic moment at the $Fe(2)^o$ site the measured[13,21,31] HF is found to be 46 T in $Sr_4Fe_4O_{11}$. This may have misled experimentalists to believe that magnetic ordering occurs for Fe^{3+} rather than Fe^{4+}. We have deduced the Fermi contact contribution to the HF from density-functional calculations. This value is found to be 17 and 30 T for the $Fe(1)^s$ and $Fe(2)^o$ sites, respectively. The larger value of HF at the $Fe(2)^o$ site reflects the higher moment at that site.

The next puzzle is the origin of the larger moment at the octahedral site than at the square-pyramidal site. If an oxygen atom is removed from a configuration with 180° Fe-O-Fe bond angle, the electrostatic repulsive force pushes the Fe atoms apart and the neighboring O atoms are collectively moved toward the vacancy to screen the repulsion. The optimized structural parameters show that the Fe atoms of the $Fe(1)^s$ site are surrounded by four base-plane O atoms at a distance of 1.87 Å compared with the Fe(1) to an apical O

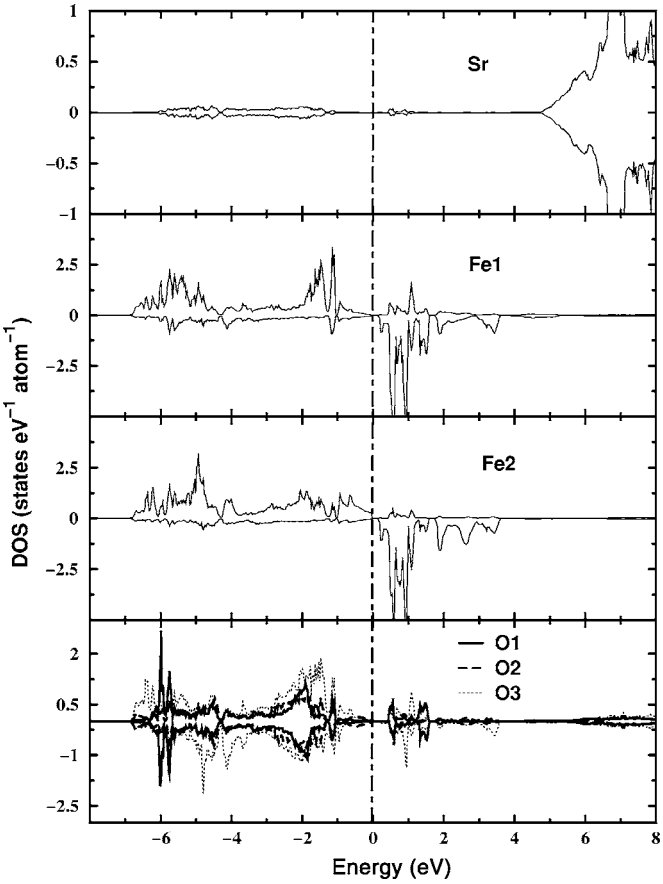

FIG. 3. Calculated site-projected density of states (DOS) for $Sr_4Fe_4O_{11}$ in the ground-state *G*-AF configuration. The Fermi level is set to zero.

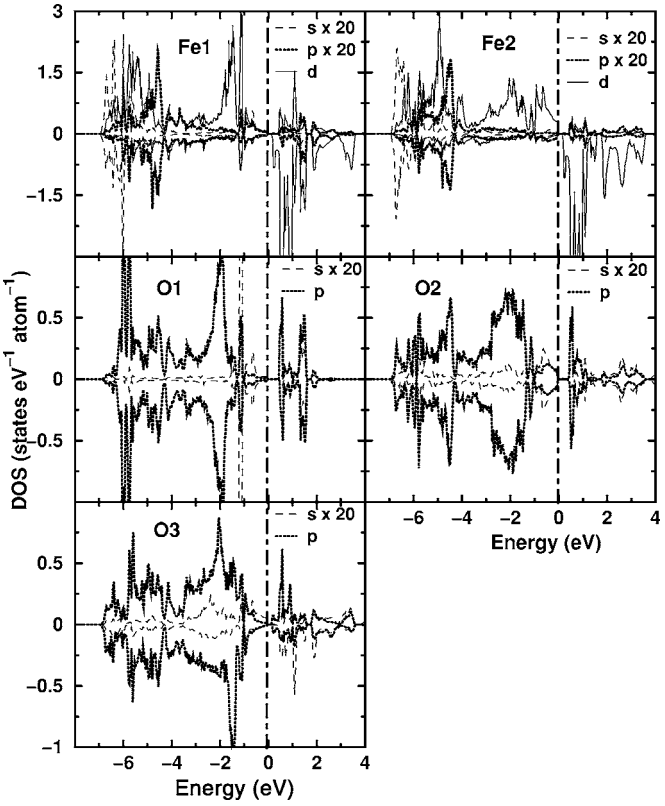

FIG. 4. Calculated *l*-projected density of states (DOS) for Fe and O atoms of $Sr_4Fe_4O_{11}$ in the ground-state *G*-AF configuration. The Fermi level is set to zero. Note that *s* and *p* states of Fe and *s* states of O are magnified by 20 times.

distance of 1.89 Å. In the $Fe(2)O_6^o$ structural subunit each Fe is surrounded by four base-plane O atoms at a distance of 2.05 Å and two apical O at a distance of 1.93 Å. These findings strongly suggest that the bonding interaction between Fe and O is stronger in the $Fe(1)O_5^s$ coordination than that in $Fe(2)O_6^o$. Hence, compared with the local surrounding of $Fe(2)O_6^o$ relatively more of the electrons in the $Fe(1)O_5^s$ subunits are participating in bonding rather than magnetism. The longer Fe-O distance in the $Fe(2)O_6^o$ subunits than that in $Fe(1)O_5^s$ indicates that the Fe 3*d* electrons in the former configuration are relatively more localized and their exchange splitting correspondingly larger than those in the $Fe(1)O_5^s$ configuration. This appears to explain why the magnetic moment at the $Fe(2)^o$ site is larger than at the $Fe(1)^s$ site.

In order to provide more insight into the bonding between the different constituents we show the site-projected DOS for $Sr_4Fe_4O_{11}$ in Fig. 3. The negligibly small DOS distribution in the valence band (VB) at the Sr site indicates pronounced ionic bonding between Sr and the other constituents. The noticeable difference in the topology of the DOS profile for the two Fe sites strongly suggests different valence states for these Fe atoms. The DOS for the minority-spin channel in the VB for both Fe sites is almost empty, indicating that these two Fe atoms are in the HS states. The broad features of the VB for the Fe sites indicate a delocalized character of these electrons and their hybridization interaction with the neighbors. The degenerate nature of the DOS for the O and Fe atoms throughout the VB strongly suggests that the bonding interaction between these atoms has a distinct covalent character. The peak feature of the DOS for $Fe(1)^s$ and O(1) around −2 eV carries the message of an appreciable covalent contribution to the $Fe(1)^s$-O bond. This could explain the relatively low moment at the $Fe(1)^s$ site. It would be interesting to understand the microscopic origin of the larger covalent participation in $Fe(1)^s$-O bond than the $Fe(2)^o$-O bond. With increasing charge and decreasing radius it is expected[18] that Fe ions will attract electron density from neighboring oxygen atoms and thus increase the electron population of its orbitals. It appears that such a mechanism can lead to an increased covalent contribution to the Fe(1)-O bonding.

In Fig. 4, *l*-projected DOS for Fe and O atoms are displayed. Since Sr-*s* electrons have a negligible presence in the VB, it has been omitted in the illustration. The *s* and *p* states of Fe sites and *s* states of O sites become visible only after significant magnification. This implies that the total DOS seen in Fig. 4 is mainly contributed by *d* states in Fe and *p* states in O atoms. The negligibly small amount of *s* and *p* states of Fe atoms is present from ~−7 to −4 eV whereas the *d* states are distributed from −7 to E_F. Similarly, the *p* states of all the three O atoms are distributed from −7 to E_F, but with noticeable differences in their topology. This implies that Fe *d* and O *p* states are strongly hybridized, how-

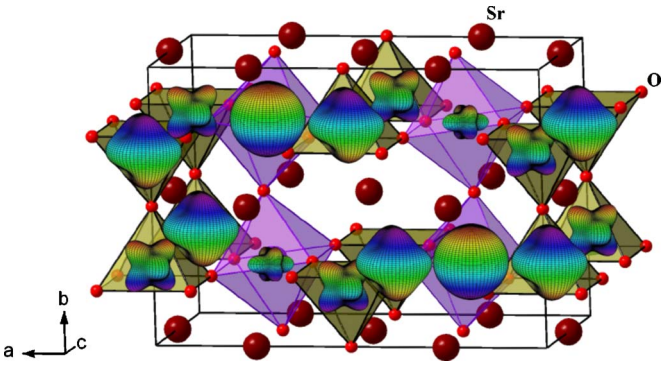

FIG. 5. (Color online) Calculated spatial distribution of valence-charge density at Fe(1)^s and Fe(2)^o for the majority- and minority-spin electrons.

ever with differences in the degree of hybridization.

In order to visualize the charge ordering in $Sr_4Fe_4O_{11}$ we present the valence d-electron density at the Fe(1)^s and Fe(2)^o sites for the majority- and the minority-spin electrons in Fig. 5. The smaller d-electron density in the minority-spin channel at the Fe(2)^o site clearly signals the HS state. The shape of the d-electron distribution at the minority-spin channel for both sites is almost the same. But the distinct topology of the distribution of d electrons at the majority-spin channel for the Fe(1)^s and Fe(2)^o sites clearly shows the different valence states of both Fe which confirms the charge ordering observed experimentally.[23] In the Fe(1)^s site, there is a considerable amount of d electrons present at the minority-spin channel also. Hence, though there are more d electrons at the Fe(1)^s than the Fe(2)^o site, the net spin density at the Fe(1)^s is smaller than that at the Fe(2)^s site. The electrons at the vicinity of the Fermi level in the VB generally participate more in the hopping interactions, and hence they are important for the exchange interaction between atoms. In Fig. 6 we show the spatial distribution for valence-band d electrons at the Fe(1)^s and Fe(2)^o sites within 1 eV from Fermi level. The interesting feature in this figure is the orientation of the d_{z^2}-like orbital along the [010] direction at the Fe(2)^o site. This clearly illuminates the superexchange interaction path. Hence, the d electrons at the Fe(2)^o form an AF alignment via O(2) (resulting in the magnetic structure given in Fig. 8). On the other hand, the valence d electrons within 1 eV from the Fermi level at the Fe(1)^s sites have a complex orbital distribution. So in spite of the bond angle for Fe(1)^s-O(1)-Fe(1)^s being 180° (which should prefer an AF interaction), the superexchange interaction is not as strong as that between Fe(2)^o. This may be one of the reasons why long-range ordering is stronger between Fe(2)^o than between Fe(1)^s sites.

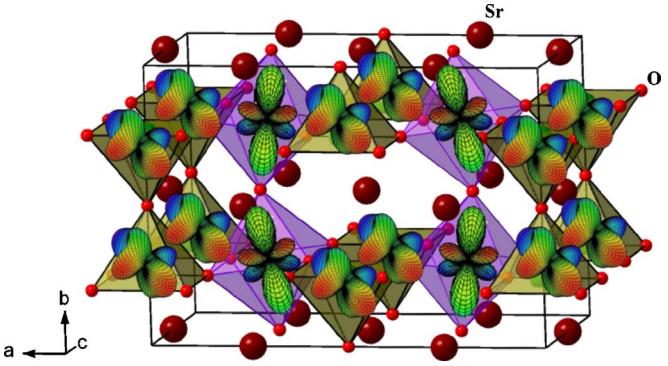

FIG. 6. (Color online) The orbital ordering pattern obtained from the occupation matrices of d states close to the Fermi level at the Fe(1)^s and Fe(2)^o sites in $Sr_4Fe_4O_{11}$.

More insight into the spin state of d electrons at the two Fe sites is also highly desirable. In an octahedral (cubic) crystal field the Fe-d levels are split into triply degenerate t_{2g} (d_{xy},d_{xz},d_{yz}) and doubly degenerate e_g $(d_{x^2-y^2},d_{z^2})$ levels. Owing to orthorhombic distortion of the octahedral coordination, the degeneracy of both t_{2g} and e_g levels is further split (see Fig. 7). With the Fe in the 4+ oxidation state there will be four d electrons to accommodate in these levels. The spin moment according to a pure ionic picture will then be $2\mu_B$ and $4\mu_B$ for low-spin (LS, $t_{2g}^4e_g^0$) and high-spin (HS, $t_{2g}^3e_g^1$) configurations, respectively. In practice, materials experience covalent hybridization between the transition-metal atoms and their surrounding atoms, which reduces the spin moment owing to the fact that some of the electrons participate in bonding rather than in magnetism. Moreover, the delocalized character of the electrons (as evident from the DOS curves in Figs. 4 and 7) reduces the exchange interaction and also the moment. So one mostly gets noninteger values for the spin moments at the transition-metal sites and noticeably induced moments at the sites of the surrounding atoms. The calculated spin moment of $3.53\mu_B$ at the Fe(2)^o site supports the inference that this site is in the 4+, HS state, as a coarse approximation. Consistent with this deduction, the calculated orbital projected DOS (Fig. 7) shows an almost negligible amount of DOS in the minority-spin channel. The magnetic structure with the long arrows at Fe sites in Fig. 8 shows long-range G-AF ordering present at the Fe(2)^o site. More details about the magnetic structure will be discussed later.

In an ideal square-pyramidal crystal field the d levels will split into doubly degenerate e_g (d_{xz},d_{yz}) nondegenerate b_{2g} (d_{xy}), a_{1g} (d_{z^2}), and b_{1g} $(d_{x^2-y^2})$ levels (see Fig. 7). With Fe^{3+} there will be five d electrons to be accommodated in these levels. The spin moment for Fe(1)^s in LS $(e_g^4b_{2g}^1a_{1g}^0b_{1g}^0)$ and HS $(e_g^2b_{2g}^1a_{1g}^1b_{1g}^1)$ configurations will then be $1\mu_B$ and $5\mu_B$, respectively, for the pure ionic case. A powder neutron diffraction study[15,24] and Mössbauer measurements[13,15,21,23,31] were unable to detect any ordered moment at the Fe(1)^s site, but according to the difference in the field-cooled and zero-field-cooled magnetic susceptibility curves[15,24] the unpaired electrons at the Fe(1)^s sites can be ferromagnetically aligned in a strong enough magnetic field. Consistent with these experimental findings a density-functional calculation gave a spin moment of $2.83\mu_B$ (for comparison, the assumed 3+, HS state in $Sr_2Fe_2O_5$ is reported[17] to exhibit a magnetic moment of $4.5\mu_B$). However, the calculated spin moment is unusually low for a 3+, HS configuration. The calculated spin moment for the Fe(1)^s site, on the other hand, is higher than for an ideal ionic 3+, LS value. Hence we have confidence in the coarse assignment of the 3+, HS state to Fe(1)^s on the additional assumption that the moment is reduced owing to the partial delocalization of the $3d$ electrons and the effect of covalence.

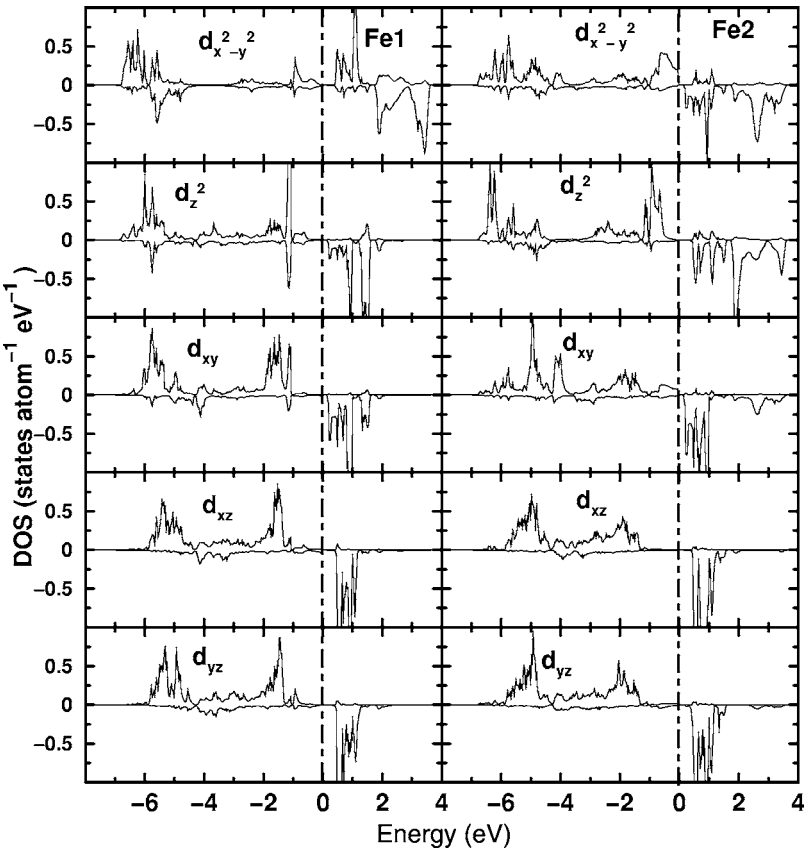

FIG. 7. Calculated orbital-projected density of states (DOS) for $Fe(1)^s$ and $Fe(2)^o$ in $Sr_4Fe_4O_{11}$ for the ground-state *G*-AF configuration. The Fermi level is set to zero.

If the $Fe(2)^o$ atom is in a 4+, HS state, one should expect Jahn-Teller distortion (JTD). But experimental and theoretical structural analyses show that neither the characteristic $LaMnO_3$-type[35] structural distortion nor the $CaFeO_3$-type[36,37] disproportionation $[2Fe^{4+}(t_{2g}^3 e_g^1) \rightarrow Fe^{4-\delta}(t_{2g}^3 e_g^{1+\delta}) + Fe^{4+\delta}(t_{2g}^3 e_g^{1-\delta})]$ characteristics of narrow-band electrons] occurs in $Sr_4Fe_4O_{11}$. As mentioned above $SrFeO_3$ is believed to provide a typical example of Fe in the 4+, HS state. However, the expected JTD is not observed for $SrFeO_3$ even at very low temperatures. The nonobservation of JTD in $SrFeO_3$ is attributed to its metallic behavior, broad-band features of the VB, and the deep-lying location of the Fe 3*d* levels. Cooperative JTD is very common for pure ionic systems with localized electrons whereas for systems with broadband features and distinct covalent characteristics JTD is not mandatory. The orthorhombic distortion of the coordination polyhedra in $Sr_4Fe_4O_{11}$ already lifts the degeneracy of the e_g levels. The $Fe(2)O_6^o$ configuration is compressed with two short (1.93 Å) and four long (2.05 Å) Fe-O bonds which is suggestive of a JTD and accordingly a HS state for $Fe(2)^o$.

It is worth analyzing the reasons behind the different conclusions for the valence and spin states for $Fe(1)^s$ and $Fe(2)^o$ arrived at from the experimental data. The room-temperature Mössbauer spectra (MS) show symmetrical doublets which were assigned to Fe^{3+} and Fe^{4+} on the basis of isomer shift, quadrupole splitting, and linewidth.[30,31] The low-saturation HF (46 T) was used to argue[31] for a low coordination of Fe^{3+} despite the fact that the isomer shift is more in line with octahedral coordination. The HF around 33 T can be interpreted as due to a 4+, HS configuration with some degree of covalence.[16,18] The observed HF value of 46 T is comparable to the 43 T field reported[38] for $Sr_2Fe_2O_5$ where Fe atoms are assigned a 3+ state. This led the experimentalists to believe that Fe^{3+} is responsible for the AF ordering in $Sr_4Fe_4O_{11}$. (Note that the HF at each site depends on the total magnetic field acting at each site.) However, the HF does not carry explicit information about the coordination number and amount of electrons at the given site. Hence, it is not possible to deduce such information from the size of the HF alone.

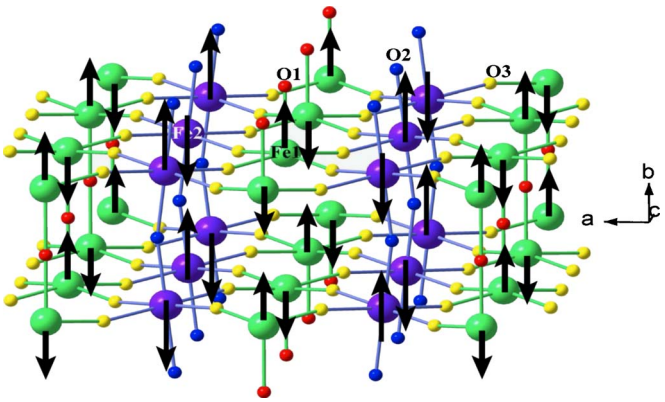

FIG. 8. (Color online) The schematic ground-state magnetic structure for $Sr_4Fe_4O_{11}$ obtained from the spin-polarized total energy calculations. The longer arrow corresponds to a moment of $3.53\mu_B$ at the $Fe(2)^o$ site and the smaller arrow reflects a moment of $2.83\mu_B$ at the $Fe(1)^s$ site. For clarity only Fe and O atoms are shown with bonds.

TABLE II. Total energy (relative to the lowest energy state in meV f.u.$^{-1}$) in $Sr_4Fe_4O_{11}$ for the para- (P), ferro- (F), and *A*-, *C*-, and *G*-type AF configurations obtained from VASP PAW calculations.

Para	Ferro	*C*-AF	*A*-AF	*G*-AF
4099.8	3865.6	757.3	127.9	0.0

The behavior of the other Fe site is unusual since no resolved magnetic splitting could be observed.[14,21,31] Based on the results from powder x-ray diffraction and MS measurements Takano *et al.*[21,32] concluded that this site is populated by Fe^{4+}, HS states with a residual disorder that is also responsible for the broad background of the MS. However, our detailed analysis (see below) indicates magnetic frustration, which is also manifested in the large difference between field-cooled and zero-field-cooled magnetic susceptibility data.[15,24] Such magnetic behavior resembles that for the observed spin-glass situation in Fe-containing perovskite-derived oxides where it is believed[39–41] that competing nearest-neighbor- and next-nearest-neighbor-exchange interactions prevent the development of long-range magnetic order.

Now we try to understand why the HF at $Fe(2)^o$ in the 4+ state is comparable with that of Fe^{3+} in $Sr_2Fe_2O_5$. The $Fe(2)^o$-O bond length is between 1.93 and 2.05 Å in $Sr_4Fe_4O_{11}$ which nearly matches that in $Sr_2Fe_2O_5$ [1.94–2.03 Å (Ref. 17)] where also Fe is in octahedral coordination. The bond length is a deciding factor for the degree of localization as well as exchange splitting and hence the magnetic moment at each site. Therefore, it is the comparable value of the Fe-O bond length and almost the same HF values in both cases that may have misled experimentalists to arrive at the wrong conclusion. It should be remembered that the valence state is decided only by the number of electrons associated with each site and not by the magnetic moment or the HF.

Magnetic structure

Magnetic exchange in perovskitelike oxides is generally assumed to take place by superexchange[42] and/or double-exchange.[43] This involves exchange between magnetic atoms via nearest-neighbor oxygen and leads to an antiparallel-parallel alignment. The reliance of the magnetic exchange upon the oxygen messenger implies that the amount and configuration of the intervening oxygen atoms should produce an alternation in the magnetic properties of a phase like $Sr_4Fe_4O_{11}$. For instance, one can imagine that oxygen vacancies will tend to decouple the interaction paths and for $Sr_4Fe_4O_{11}$ in particular lead to the introduction of an equal amount of Fe^{3+} and Fe^{4+} which in turn also would result in the formation of ferromagnetic (F) double exchange.

According to the size of the interplane and intraplane exchange interactions in perovskitelike materials one often arrives at F-, *A*-AF-, *C*-AF-, or *G*-AF-type ordering.[44] In order to arrive at the ground-state spin arrangement in $Sr_4Fe_4O_{11}$ we made total-energy calculations for the just mentioned different magnetic configurations. The calculated total energy for $Sr_4Fe_4O_{11}$ in these different spin configurations relative to the *G*-AF-type ground state (Table II) shows that large amounts of energy are gained when AF ordering is introduced. The *G*-AF-type spin arrangement represents the ground state for $Sr_4Fe_4O_{11}$ whereas *A*-AF-type ordering occurs at only 128 meV f.u.$^{-1}$ higher energy than the *G*-AF configuration and this is associated with the possibility of having a double-exchange interaction via $Fe(2)^o$-O(3)-$Fe(1)^s$ within the plane. The calculated spin moments do not differ much between the different Fe sites for the different spin configurations (see Table III). In particular it should be noted that we always arrived at a smaller moment at the $Fe(1)^s$ site than the $Fe(2)^o$ site. Relatively large spin moments (around $0.17\mu_B$) were found at all the oxygen sites for the F configuration, which result in a much higher value for the total spin moment than the sum of the spin moments at the $Fe(1)^s$ and $Fe(2)^o$ sites.

TABLE III. Calculated spin moment (in μ_B per Fe atom) for $Sr_4Fe_4O_{11}$ in the F and AF phases. "Total" refers to the total spin moment (in μ_B per formula unit).

Configuration	Fe(1)	Fe(2)	Total
F	2.78	3.26	13.92
A-AF	3.00	3.49	0.0
C-AF	2.80	3.30	0.0
G-AF	2.91	3.57	0.0
G-AF (FP-LAPW)	2.83	3.53	0.0
Expt.[a]		3.55	0.0
Expt.[b]		3.3	0.0

[a]Reference 15.
[b]Reference 24.

The Mössbauer spectroscopic[13,15,21,31] and PND measurements[14,15,24] indicated that only one sublattice orders antiferromagnetically. The observed magnetic reflections of the PND patterns were refined according to the spin models described in the Shubnikov groups $Cm'm'm'$ and $Cmm'm'$.[15] In the $Cm'm'm'$ model the moments of $Fe(1)^s$ are aligned along the [010] direction where the AF coupling is facilitated by a superexchange interaction via O(1) whereas in $Cmm'm'$ spin moments are permitted on both $Fe(1)^s$ and $Fe(2)^o$ sites. In the present calculations we arrived at the latter arrangement (see Fig. 8). In this spin configuration the superexchange interactions take place via both O(1) and O(2) atoms. However, according to the observed magnetic PND reflections (as well as the Mössbauer spectroscopic data) only the moment at the $Fe(2)^o$ site is ordered whereas that at $Fe(1)^s$ should be be zero. If the moment on the $Fe(1)^s$ site is zero and that at $Fe(2)^o$ is constrained to be along [010], any of the AF configurations in Table III would most likely be facilitated by superexchange interactions via the O(2) atom.

Hodges *et al.*[14] placed Fe^{4+} and Fe^{3+} in $F(1)^s$ and $F(2)^o$ sites, respectively (based on bond-valence arguments), which favor the magnetic arrangement according to the Shubnikov group $Cmm'm'$. Schmidt *et al.*[15] considered that a bond-valence sum for individual sites of complex oxides is not

meaningful and criticized the proposed magnetic structure. Moreover, Schmidt *et al.* argued that the Fe^{4+} valence state in Sr-Fe-O compounds has so far only been established for octahedral sites[13,45–47] and thus they concluded that Fe^{3+} takes the $F(1)^s$ site and Fe^{4+} the $F(2)^o$ site. This assignment favors the *Cm′m′m′*-based model, but Schmidt *et al.* nevertheless claim that "the conclusions drawn from this particular model can be easily be applied to the *Cmm′m′* model since the $Fe(1)^s$ and $Fe(2)^o$ sublattices have similar topology." It should be noted that the refined moments from both models are of almost equal values.

The magnetic structure for $Sr_4Fe_4O_{11}$ illustrated in Fig. 8 suggests strong AF $Fe(2)^o$-O-$Fe(2)^o$ superexchange interactions within the one-dimensional chains of the vertex-linked $Fe(2)O_6^o$ octahedra along [010] (see also Fig. 6). There are no throughout $Fe(2)^o$-O-$Fe(2)^o$ interaction paths within the *ac* planes, whereas weak $Fe(2)^o$-O-O-$Fe(2)^o$ interaction paths appear to provide an exchange path which is able to account for the observed magnetic ordering. Our calculations show that the apical oxygens at both octahedral and square-pyramidal sites carry sizable spin moments of around $0.13\mu_B$. Although the interatomic distance between the apical oxygen and the $Fe(2)^o$ is shorter than the distance between $Fe(2)^o$ and the oxygen in the base, the apical oxygens carry a larger spin moment. This may be another indication of a superexchange path via apical oxygen atoms (a similar conclusion is arrived at also from the orbital ordering analysis discussed above). This appears to explain why we have AF exchange interactions between $Fe(2)^o$ along [010].

Even though our calculations show a spin moment of $2.83\mu_B$ at the $Fe(1)^s$ site, both PND[15,24] and MS measurements[14,21,31] were unable to confirm a cooperative magnetic moment at that site. What can possibly be the microscopic origin behind this behavior? Each $Fe(1)^s$ is surrounded by four nearest-neighbor $Fe(2)^o$ atoms within the *ac* planes, for which two of the resulting $Fe(1)^s$-O(3)-$Fe(2)^o$ exchange paths couple ferromagnetically and the remaining two are AF. Hence, the magnetic moments at the $Fe(1)^s$ site become topologically frustrated when exposed to the interactions in the *G*-AF-type $Fe(2)^o$ sublattice. Therefore, the experiments have been unable to find any long-range magnetic ordering for the $Fe(1)^s$ sites.

Then it is pertinent to ask why the $Fe(2)^o$ sites are the first to order moments antiferromagnetically [instead of $Fe(1)^s$ moments]. The $Fe(1)^s$-O(1)-$Fe(1)^s$ angle is exactly 180° which would favor AF superexchange interactions between the $Fe(1)^s$ moments along [010] (viz., the "bow-ties" between every four octahedra chains along the *b* axis would experience AF ordering). The size of the magnetic moment at the $Fe(2)^o$ site is larger than that at the $Fe(1)^s$ site and hence the exchange interaction between the $Fe(2)^o$ atoms will be larger than that between the $Fe(1)^s$ atoms. Consistent with this viewpoint the calculated Lichtenstein's exchange interaction parameter (J_{ij}) from the tight-binding linear MT orbital (TB-LMTO) program came out as 56 meV, between the Fe(2) atoms, and it is higher compared with that between Fe(1) atoms (41 meV). This simple estimate also suggests that the $Fe(2)^o$ moments should order first.

The total-energy calculations show that among the considered magnetic configurations, the *G*-AF-type ordering represents the ground state for $Sr_4Fe_4O_{11}$. We have made additional total-energy calculations for the magnetic configuration where $Fe(1)^s$ is nonmagnetic (in an attempt to mimic some of the experimental interpretations) and $Fe(2)^o$ exhibits *G*-AF-type ordering. Interestingly this configuration was found to stabilize with good convergence but at 1.85 eV $f.u.^{-1}$ higher energy than the ground-state configuration. Hence, theory rules out the possibility of a nonmagnetic situation for $Fe(1)^s$ in $Sr_4Fe_4O_{11}$. We believe that it is the competition between the F and AF interactions in the $Fe(1)^s$ sublattice [viz., AF superexchange interaction for $Fe(1)^s$-O(1)-$Fe(1)^s$ and F double-exchange interaction for $Fe(1)^s$-O(3)-$Fe(2)^o$] which creates the frustration, resulting in the nonobservation of long-range magnetic ordering at the $Fe(1)^s$ site. As a result, $Sr_4Fe_4O_{11}$ can be regarded as a "phase-separated system with two phases, one represented by *G*-AF-type ordered $Fe(2)O_6^o$ units in a $SrFeO_3$-like sublattice and the other consisting of a spin-glass-like magnetically ordered $Fe(1)O_5^s$ units in a $Sr_2Fe_2O_5$-like sublattice."

As a summary, the magnetic structure of $Sr_4Fe_4O_{11}$ can be visualized as follows. Below T_N=230 K, the $Fe(2)^o$ sublattice forms an AF spin structure, with magnetic coupling mediated by $Fe(2)^o$-O(2)-$Fe(2)^o$ superexchange interactions parallel to the [010] direction and $Fe(2)^o$-O(3)-O(3)-$Fe(2)^o$ super-superexchange interactions within the *ac* planes. Each $Fe(1)^s$ will then have two $Fe(2)^o$ neighbors with "up-spin magnetic moment" and two with "down-spin magnetic moment." Irrespective of whether the $Fe(1)^s$-O-$Fe(2)^o$ superexchange interactions are F or AF, the Fe(1) magnetic moments will be topologically frustrated due to the opposite spin alignments of the nearest-neighbor $Fe(2)^o$ atoms, resulting in no long-range order in reality.

V. CONCLUSIONS

The optimized structural parameters for $Sr_4Fe_4O_{11}$ are found to be in good agreement with the low-temperature powder-neutron-diffraction results. Although the powder-neutron-diffraction and Mössbauer spectroscopic measurements are unable to show magnetic moment at one of the Fe sites, field-cooled and zero-field-cooled magnetic susceptibility data suggest that both Fe sites carry significant magnetic moments. Using accurate density-functional calculations we have shown that there are indeed large magnetic moments at both the Fe sites. As the calculations show large magnetic moments at the octahedral Fe(1) site, the nonobservation of long-range magnetic ordering of the Fe(1) moments must be associated with a spin-glass-like behavior. The origin of the magnetic frustration in $Sr_4Fe_4O_{11}$ has been analyzed. Among the experimentally reported different possibilities, the present calculations suggest that the (formal) Fe^{3+} are in the square-pyramidal sites and (formal) Fe^{4+} species take the octahedral sites (both valence assignments are to be regarded as coarse approximation). The spin state for the formal Fe^{4+} can be assigned as HS and the calculated spin moment for the formal Fe^{3+} site is higher than for a LS

spin and lower than for a HS state. Within the experimentally suggested magnetic structures based on Shubnikov groups *Cmm′m′* and *Cm′m′m′*, we confirm that *Cmm′m′* is more appropriate to describe the magnetic structure. The unusual magnetic properties of $Sr_4Fe_4O_{11}$ can be related to the crystal structure and charge order of the iron species.

ACKNOWLEDGMENTS

The authors are grateful for the financial support from the Research Council of Norway. Part of these calculations were carried out at the Norwegian supercomputer facilities.

*Electronic address: vidya.revindran@kjemi.uio.no; URL: http//folk.uio.no/revindrv

[1] B. C. H. Steele, Mater. Sci. Eng., B **13**, 79 (1992).
[2] H. Y. Tu, N. Imanishi, and O. Yamamoto, Solid State Ionics **100**, 283 (1997).
[3] M. L. Post, J. J. Tunney, D. Yang, X. Du, and D. L. Singleton, Sens. Actuators B **59**, 190 (1999).
[4] L. Qiu, T. H. Lee, L.-M. Liu, Y. L. Yang, and A. Jacobson, Solid State Ionics **76**, 321 (1995).
[5] C. H. Chen, H. J. M. Bouwmeester, R. H. E. van Doorn, H. Kruidhof, and A. J. Burggraaf, Solid State Ionics **98**, 7 (1997).
[6] S. Pei, M. S. Kleefisch, T. P. Kobylinski, J. Faber, C. A. Udovich, V. Zhang-McCoy, B. Dabrowski, U. Balachandran, R. L. Mieville, and R. B. Poeppel, Catal. Lett. **30**, 201 (1995).
[7] C. Schinzer, R. A. Saymeh, and H. M. Asfour, Z. Naturforsch., B: Chem. Sci. **52**, 927 (1997).
[8] C. E. Mohn, N. L. Allan, C. L. Freeman, P. Ravindran, and S. Stølen, Phys. Chem. Chem. Phys. **6**, 3052 (2004).
[9] B. C. H. Steele, Curr. Opin. Solid State Mater. Sci. **1**, 684 (1996).
[10] M. Takano and Y. Takeda, Bull. Inst. Chem. Res., Kyoto Univ. **61**, 406 (1983).
[11] R. Vidya, P. Ravindran, P. Vajeeston, A. Kjekshus, and H. Fjellvåg, Phys. Rev. B **69**, 092405 (2004).
[12] R. Vidya, P. Ravindran, A. Kjekshus, and H. Fjellåg (unpublished).
[13] Y. Takeda, K. Kanno, T. Takeda, O. Yamamoto, M. Takano, N. Nakayama, and Y. Bando, Solid State Chem. **63**, 237 (1986).
[14] J. P. Hodges, S. Short, J. D. Jorgensen, X. Xiong, B. Dabrowski, S. M. Mini, and C. W. Kimball, J. Solid State Chem. **151**, 190 (2000).
[15] M. Schmidt, M. Hofmann, and S. J. Campbell, J. Phys.: Condens. Matter **15**, 8691 (2003).
[16] P. K. Gallagher, J. B. MacChesney, and D. N. E. Buchanan, J. Chem. Phys. **41**, 2429 (1964).
[17] M. Schmidt and S. J. Campbell, J. Solid State Chem. **156**, 292 (2001).
[18] J. B. MacChesney, R. C. Sherwood, and F. Potter, J. Chem. Phys. **43**, 1907 (1965).
[19] T. Takeda, Y. Yamaguchi, and H. Watanabe, J. Phys. Soc. Jpn. **33**, 967 (1972).
[20] J.-C. Grenier, N. Ea, M. Pouchard, and P. Hagenmuller, J. Solid State Chem. **58**, 243 (1985).
[21] M. Takano, T. Okita, N. Nakayama, Y. Bando, Y. Takeda, O. Yamamoto, and J. B. Goodenough, J. Solid State Chem. **73**, 140 (1988).
[22] B. C. Tofield, C. Greaves, and B. E. F. Fender, Mater. Res. Bull. **10**, 737 (1975).
[23] L. Fournes, Y. Potin, J. C. Grenier, G. Demazeau, and M. Pauchard, Solid State Commun. **62**, 239 (1987).
[24] H. Fjellvåg, O. H. Hansteen, Y. Bréard, and B. C. Hauback (unpublished).
[25] P. E. Blöchl, Phys. Rev. B **50**, 17953 (1994).
[26] G. Kresse and J. Furthmuller, Comput. Mater. Sci. **6**, 15 (1996).
[27] J. P. Perdew, K. Burke, and M. Ernzerhof, Phys. Rev. Lett. **77**, 3865 (1996).
[28] P. Ravindran, R. Vidya, A. Kjekshus, H. Fjellvåg, and O. Eriksson (unpublished).
[29] P. Blaha, K. Schwarz, G. K. H. Madsen, D. Kvasnicka, and J. Luitz, Computer code WIEN2k, revised edition 2001, an augmented plane waves+local orbitals program for calculating crystal properties, Vienna, Vienna University of Technology, 2003.
[30] T. C. Gibb, J. Mater. Chem. **4**, 1445 (1994).
[31] T. C. Gibb, J. Chem. Soc. Dalton Trans. **4/1629**, 1455 (1985).
[32] M. Takano, N. Nakanishi, Y. Takeda, and T. Shinjo, in *Ferrites, Proceedings of the International Conference, Kyoto, Japan, 1980*, edited by H. Watanabe, S. Iida, and M. Sugimoto (Center for Academic Publication, Tokyo, Japan, 1981), p. 389.
[33] J. Ziolkowski, J. Solid State Chem. **57**, 269 (1985).
[34] S. Nakamura and S. Iida, Jpn. J. Appl. Phys., Part 2 **34**, L291 (1995).
[35] J. B. Goodenough, Phys. Rev. **100**, 564 (1955).
[36] J. B. Goodenough, J. Solid State Chem. **12**, 148 (1975).
[37] M. Takano, N. Nakanishi, Y. Takeda, S. Naka, and T. Takada, Mater. Res. Bull. **12**, 923 (1977).
[38] P. D. Battle, T. C. Gibb, and S. Nixon, J. Solid State Chem. **79**, 75 (1989).
[39] R. Rodriguez, A. Fernandez, A. Isalgue, J. Rodriguez, A. Labarta, J. Tejada, and X. Obradors, J. Phys. C **18**, L401 (1985).
[40] P. D. Battle, T. C. Gibb, A. J. Herod, and J. P. Hodges, J. Mater. Chem. **5**, 75 (1995).
[41] P. D. Battle, T. C. Gibb, A. J. Herod, S. H. Kim, and P. H. Munns, J. Mater. Chem. **5**, 865 (1995).
[42] P. W. Anderson, Phys. Rev. **79**, 350 (1950).
[43] C. Zener, Phys. Rev. **82**, 403 (1951); P. W. Anderson and H. Hasegawa, *ibid.* **100**, 675 (1955); P. G. de Gennes, *ibid.* **118**, 141 (1960).
[44] P. Ravindran, A. Kjekshus, H. Fjellvåg, A. Delin, and O. Eriksson, Phys. Rev. B **65**, 064445 (2002).
[45] S. E. Dann, M. T. Waller, and D. B. Currie, J. Solid State Chem. **92**, 237 (1991).
[46] S. E. Dann, M. T. Waller, and D. B. Currie, J. Solid State Chem. **97**, 179 (1992).
[47] S. E. Dann, M. T. Waller, D. B. Currie, M. F. Thomas, and A. D. Al-Rawwas, J. Mater. Chem. **3**, 1231 (1993).